Microchemical Journal 99 (2011) 429–438

Contents lists available at ScienceDirect

Microchemical Journal

journal homepage: www.elsevier.com/locate/microc

Evaluation of airborne particles at the Alhambra monument in Granada, Spain

Benjamin Horemans [a,*], Carolina Cardell [b], László Bencs [a,c], Velichka Kontozova-Deutsch [a], Karolien De Wael [a], René Van Grieken [a]

[a] Environmental Analysis Group, Department of Chemistry, University of Antwerp, Universiteitsplein 1, BE-2610 Antwerp, Belgium
[b] Department of Mineralogy and Petrology, University of Granada, Campus Fuentenueva s/n, 18071 Granada, Spain
[c] Research Institute for Solid State Physics and Optics, Hungarian Academy of Sciences, P.O. Box 49, H-1525 Budapest, Hungary

ARTICLE INFO

Article history:
Received 10 June 2011
Accepted 19 June 2011
Available online 25 June 2011

Keywords:
Alhambra monument
Energy dispersive X-ray fluorescence spectrometry
Ion chromatography
Suspended particulate matter
PM_{10}
PM_1
Cultural heritage
Preventive conservation

ABSTRACT

As a part of an ongoing investigation regarding the air quality at the Alhambra monument (UNESCO World Cultural Heritage), indoor and outdoor atmospheric aerosols (PM_1 and PM_{10-1}) and pollutant gases (O_3, NO_2, SO_2 and NH_3) were studied during summer and winter. Bulk elements, ionic compounds and black carbon (BC) in aerosols were analyzed with X-ray fluorescence spectrometry, ion chromatography and aethalometry/reflectometry, respectively. Natural PM_{10-1} aerosols, such as carbonate-rich soil and sea salts, reacted with a typical urban atmosphere, producing a mixture of particulates with diverse chemical composition. The content/formation of secondary inorganic aerosols depended on the air temperature and absolute humidity. Ratios of typical mineral elements (i.e., Ti/Fe and Si/Fe) showed that Saharan dust events contribute to the composition of the observed mineral aerosol content. BC, V and Ni originated from diesel exhaust, while Cu, Cr, Pb and Zn came mainly from non-exhaust vehicular emissions. Weathering phenomena, such as blackening and pigment discoloration, which could arise from gradual aerosol deposition indoors, are discussed.

1. Introduction

Deterioration of cultural heritage exposed to atmospheric gases and airborne particulate matter (PM) receives an increasing attention nowadays [1]. In order to protect and conserve the relics of human history, it is important to understand how atmospheric pollutants interact with cultural heritage items (CHIs). Although wet and dry deposition of gases and aerosols to monuments are complex processes, several studies have evaluated soiling in a quantitative way by means of particle deposition rates [2–6].

For many years, SO_2 has been considered as the main atmospheric pollutant, which poses a corrosion risk to artworks. On the other hand, reactions between the heritage materials and deposited particles can drastically affect the morphology, composition, strength and aesthetic appearance of CHIs [7]. Furthermore, the effect of SO_2 on materials is often a synergistic process, which involves the action of particulate pollutants too [8,9]. Since SO_2 emissions have drastically decreased for the past decades, the focus on preventive conservation is shifting towards other reactive gases, such as HNO_3 and O_3 [10–12]. Although the emission of NH_3 has decreased for several European countries, for Spain, its substantial increase over the last 20 years has been estimated [13]. Although NH_3 has no direct effect on any material, it is a precursor gas for secondary inorganic aerosols (SIA), which can contribute to the weathering of CHIs.

Most monuments worldwide are located in urban environments, where pollution, originating from domestic heating, construction works, traffic and industry, has harmful effects to buildings and decorative materials [14]. Black crust formation, material decohesion and dust deposition often occurs on the exterior of the buildings, causing undesirable aesthetic effects. Inside monuments, soiling and chemical weathering of CHIs can occur due to both indoor and outdoor phenomena. At present, the strategy to safeguard CHIs is to elaborate preventive conservation measures, which require the knowledge of diverse climatic and atmospheric parameters connected to them. Thus, monitoring of air pollutants and microclimatic parameters are generally performed in order to identify possible threats to conservation [15,16].

The world famous Alhambra monument brings every year more than 3 million people to Granada in Southern Spain. This unique piece of Islamic architecture has been listed as UNESCO world cultural heritage since 1984. Until now, the atmospheric risks to its conservation have not yet been evaluated, although the urbanization of Granada and the immense pressure of mass tourism raise concerns of preventive conservators. In this work, the indoor and outdoor air quality at the Alhambra monument is studied by the application of complementary analytical chemical techniques with the aim of formulating a strategy for its preventive conservation.

* Corresponding author. Tel.: +32 32652381; fax: +32 32652376.
E-mail address: benjamin.horemans@ua.ac.be (B. Horemans).

0026-265X/$ – see front matter © 2011 Elsevier B.V. All rights reserved.
doi:10.1016/j.microc.2011.06.018

2. Experimental

2.1. Description of the sampling sites

At the feet of the Sierra Nevada Mountains in Southeast Spain, at about 800 m above the mean sea level, the Alhambra monument overlooks the city of Granada on top of the Sabika hill. The city with a population of 300000 is situated in a natural basin surrounded by mountains with altitudes up to 3500 m. It is around 50 km of the Mediterranean Sea and approximately 200 km of the African continent. The region has a near-continental climate with cool/wet winters, hot summers and high diurnal temperature variability.

The Alhambra represents the grandest and finest example of Islamic art and architecture from the Middle Ages still standing in the Western world. The Alhambra was a fortified palatial citadel, whose construction took from the 11th to the 15th century, with the most outstanding palaces built during the Nasrid dynasty (1238–1492). The Alhambra is surrounded by three concentric walls and includes 23 towers, four gates, seven palaces, a fortress, public and private mosques and spas, etc. (Fig. 1). All the visitors have to leave their vehicles in the parking lot of the monument at the Southeastern wall, from where they have to proceed on foot. Public transport buses are scheduled every 10–15 min to shuttle the annual 3 million visitors between the city and the monument.

The traditional access to the Alhambra from the city center was via Cuesta Gomerez passing through the renaissance (1536) Pomegranates gate and the Alhambra park (Fig. 1). Due to the intense deterioration of this gate, a restoration program started in April 2007. Therefore, the cityhall temporarily closed this entry to the Alhambra to traffic. These works finished in January 2010. During this time-span, air-quality research was solicited by the Patronato de la Alhambra prior to reopening to traffic. To this end, atmospheric aerosols were analyzed in Cuesta Gomerez (K2) and the Alhambra palaces and compared with those measured in Cuesta del Chapiz (K1), a busy traffic access to the Albayzin (UNESCO world cultural heritage since 1984), also on a steep slope.

In the palaces, sampling campaigns were conducted at three locations, each chosen on the base of their architectural characteristics and artistic values. The first site was the 'Hall of the two Sisters' (P1), a semi-open room that surrounds the famous 'Courtyard of the Lions'. The 'Royal Baths' (P2) were chosen as a second sampling site, since they form an enclosed area, which is always considerably cooler and more humid compared to other sections of the palaces. The 'Hall of the Ambassadors' (P3), the main hall of the Comares palace, is a room with a huge open entrance and windows covered with wooden artworks, and was chosen as a third indoor sampling site.

2.2. Sampling strategy

A summer (15th of June until 5th of July 2009) and a winter (1st until 10th of February 2010) campaign was conducted in order to compare the atmospheric pollution under typical meteorological conditions (Table 1). Two types of MS&T™ samplers (Air Diagnostics and Engineering Inc., Harrison, ME, USA) were used to collect aerosol fractions with an equivalent aerodynamic diameter (EAD) below 1 μm (PM_1) and 10 μm (PM_{10}) on Teflon membrane filters (TK15-G3M 37 mm, Pall, Ann Arbor, MI, USA). The vacuum pumps for PM_1 and PM_{10} sampling (Air Diagnostics and Engineering Inc.) were operated at flow-rates of 23 and 10 l min^{-1}, respectively, which was checked daily with a calibrated rotameter. Total sampled air volumes were registered with standard gas-flow meters. Black carbon (BC) was monitored with a dual-channel, portable aethalometer (AE42, Magee Scientific, Berkeley, CA, USA) every 10 min. Since no electricity was available during the closing hours of the monument, car batteries were used as a power supply for the sampling equipment. During daytime, they were recharged in order to ensure the next 24 h operation cycle.

During the summer campaign, one set of samplers was placed as an outdoor 'reference' (R1), and another moved together with the aethalometer between P1, P2 and P3 (Fig. 1). During the winter campaign, PM_1 and PM_{10} were collected concurrently at P1, P2 and P3 sites. The aethalometer was applied at the K1 (days 1–7) and K2 (days 8–10) sites, together with additional MS&T PM_{10} and PM_1 samplers. All samples (gaseous and aerosol) were transported in sealed containers and stored in a fridge at 4 °C until processing.

Gaseous air pollutants (NO_2, SO_2, NH_3 and O_3) were sampled simultaneously at each site with passive diffusion tubes (Radiëllo, Padova, Italy). For each gas, 2–4 samples were collected concurrently. The micro-climate was monitored at each site with ATX-11 data

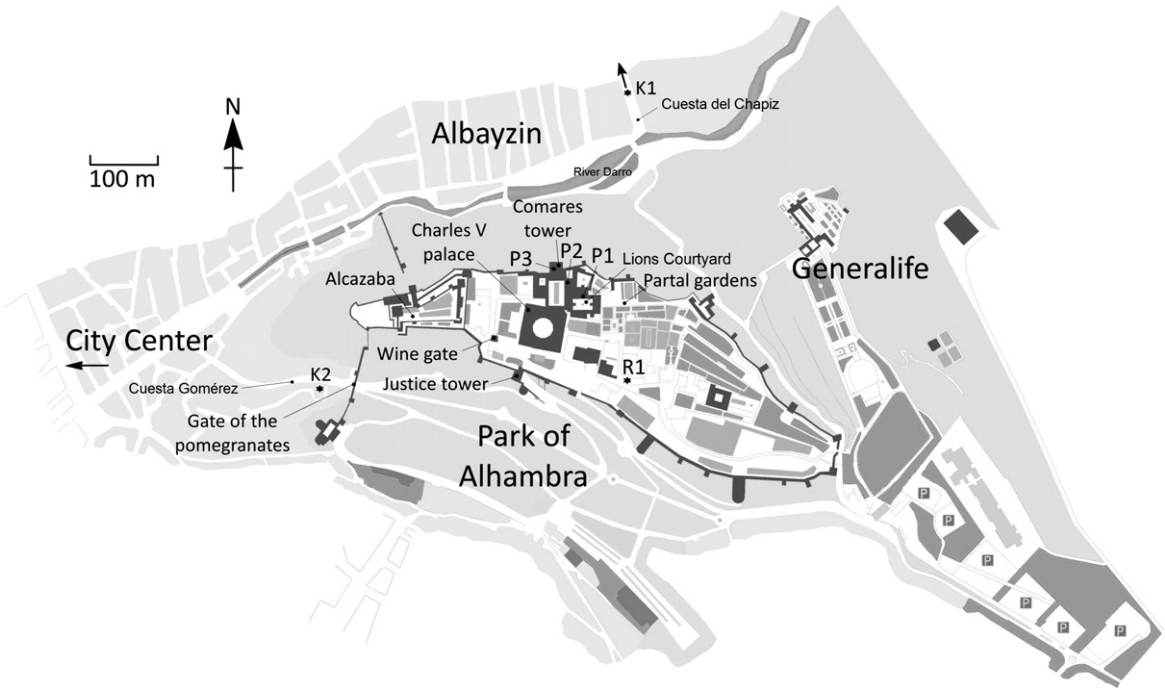

Fig. 1. Map of the Alhambra monument with the sampling sites – P1: the Hall of the two Sisters (s, w); P2: Royal Baths (s, w); P3: Hall of the Ambassadors (s, w); R1: reference site (s); K1: Cuesta del Chapiz (w); K2: Cuesta de Gomérez (w) – (s)ummer; (w)inter.

Table 1
Daily meteorological conditions during the summer and the winter campaigns.

Statistic	Air temperature[a]	Relative humidity[a]	Wind speed[b]	Solar radiation[b]	Precipitation[c]
	(°C)	(%)	(m s^{-1})	(MJ m^{-2})	(mm)
Summer: 15/06-05/07/2009 (n = 21)					
25th percentile	24	40	0.8	25	0.0
50th percentile	25	43	0.9	28	0.0
75th percentile	25	46	0.9	29	0.0
Max.	26	49	1.3	30	0.0
Min.	22	37	0.6	16	
Abs. max.	28	60	7.7		
Abs. min.	20	25			
Winter: 01/02-10/02/2010 (n = 7)					
25th percentile	7.5	75	0.5	5	0.0
50th percentile	7.7	83	0.6	9	1.0
75th percentile	8.0	88	0.8	11	8.5
Max.	8.3	93	1.0	14	23.0
Min.	4.3	68	0.5	3	
Abs. max.	9.6	97	6.9		
Abs. min.	4	56			

[a] Average values for three sites in the Nasrid palaces (P1, P2, P3; Fig. 1).
[b] Taken from a station (Pinos Puente) of the Spanish regional agro-climatic information network located just outside the city of Granada at about 16 km northwest of the Alhambra monument.
[c] Collected at a site in the Albayzin close to K1.

loggers (ATAL, Purmerend, The Netherlands), which registered the air temperature and the relative humidity (RH) every 15 min.

2.3. Analytical methodology

Before and after sampling, filters were conditioned for 48 h in a clean and climate controlled room ($T = 20 \pm 1$ °C, $RH = 50 \pm 5\%$), followed by gravimetric analysis on a MX5 microbalance (accuracy: 1 μg, Mettler Toledo, Columbus, OH, USA). The collected amount of aerosol was calculated from the mass difference of each filter before and after sampling.

Energy-dispersive X-ray fluorescence (EDXRF) spectrometry and ion chromatography (IC) were applied to determine the concentrations of 16 elements and 8 major ions on the aerosol loaded filters, respectively. Detailed description on the analytical equipment and procedures can be found elsewhere [17,18]. The analytical performance data of the methods are summarized in Table 2.

In order to have an estimate of the BC concentration at the palaces during winter (no aethalometer was applied), reflection measurements were performed by an EEL 043 smoke stain reflectometer (Diffusion Systems Ltd., London, UK). The estimation is based on the relationship between BC and the reflection of an aerosol loaded filter [19]:

$$BC\left(\mu g\, m^{-3}\right) = 6.02 \times 10^4 \times n \times (\delta / 2) \times \ ln(R_0/R) \quad (1)$$

where R_0/R is the reflectance of a white-light beam on a blank filter to that of a sampled filter, and δ is the optical depth of the sampled air column (m^{-1}). By convention, the constant n equals to 2, when using white light and Whatman No. 1 filter papers [20]. For the present filter media, n was determined in an iterative way, in order to have the highest correlation (r) and maximum overlap (minimal $\chi^2 = \Sigma_i(x_i - y_i)^2$) between the BC concentrations obtained by reflection measurements and aethalometry (data for both techniques were available at K1 and K2). A value of $n = 3.5$ was found to be optimal ($\chi^2 = 4.8$; $r = 0.995$; $y = 1.34\, x - 2.15$).

IC was used for the quantification of NO_2, SO_2 and NH_3 by analyzing the water extracts of gaseous samplers for NO_3^-, SO_4^{2-} and NH_4^+, respectively. O_3 was determined with a colorimetric method as recommended by Radiëllo [21]. The detection limits of NO_2, SO_2, NH_3 and O_3 were found to be 0.6, 0.9, 1 and 2 μg m^{-3}, respectively. Based on parallel determinations, the overall uncertainty of the method was estimated to be better than 20%.

Table 2
Analytical performance data of the EDXRF and IC methods.

	U_{QL}[a] (%)	DL (ng m^{-3})[b]		$n_{DL}\|n_{QL}$[c]			
		PM_1	PM_{10}	PM_1		PM_{10}	
				S[d]	W[d]	S	W
EDXRF							
Al	10	13	30	14|6	2|1	39|39	28|14
Pb	14	2	4	36|34	27|23	39|36	30|24
Ca	5	2	5	39|39	38|19	39|39	38|38
Cl	7	3	7	1|1	30|19	39|32	38|35
Cr	n.a.	1	3	2|0	1|0	31|0	14|1
Cu	7	2	5	35|35	22|19	39|37	32|24
Fe	6	1	3	39|39	38|31	39|39	38|38
K	5	2	6	39|39	38|38	39|39	38|38
Mn	11	1	3	35|4	25|2	39|38	30|11
Ni	9	0.6	1	37|33	38|23	35|26	37|14
S	5	2	4	39|39	38|38	39|39	38|38
Si	7	8	19	31|16	5|4	39|39	37|36
Sr	10	0.9	2	9|2	2|0	39|37	24|7
Ti	8	0.7	2	18|10	6|1	39|39	37|27
V	14	0.3	0.7	39|35	38|27	39|37	38|29
Zn	8	2	4	33|7	32|14	39|29	36|17
IC							
Ca^{2+}	12	22	51	38|35	20|6	38|38	33|22
Cl^-	11	3	8	4|2	19|13	39|32	38|37
K^+	4	68	156	38|38	8|1	38|38	6|0
Mg^{2+}	17	0.5	1	38|33	29|25	38|38	35|34
Na^+	6	9	20	38|26	36|21	38|38	38|34
NH_4^+	5	2	1	38|38	38|38	32|38	38|38
NO_3^-	5	8	19	39|21	38|38	39|39	38|38
SO_4^{2-}	5	8	19	39|39	38|38	39|39	38|38

[a] Uncertainty for results above the quantification limit ($10 \times SD_{blank}$) which incorporates all errors introduced during sampling, analysis, and the calculation of concentrations in air.
[b] Detection limit ($3 \times SD_{blank}$) calculated for a theoretical sampling period of 24 h. Due to variations in real sampling periods (±4 h) the DL for individual samples could deviate from these entries by maximally 17%.
[c] Number of detects | number of quantified results.
[d] (S)ummer: $n_{total} = 39$; (W)inter: $n_{total} = 38$.
n.a. – not applicable.

2.4. Statistical methods and models

Non-detectable concentrations of elements and ions were replaced by one-half of the value of the detection limit (DL). For results in the PM_{10-1} fraction (i.e., $PM_{10} - PM_1$), the DL of PM_{10} was used, i.e. the highest of both. All correlations were evaluated on the base of Pearson correlation coefficients (r) with a two-tailed test of significance (p). Factor analysis was performed with the principal component extraction method (eigenvalues > 1) and Varimax rotation. The difference between two averages was made statistically sound by an independent student *t*-test, assuming equal, or unequal variances. The equality of variances was evaluated by an F-test. In order to evaluate the intrusion of North African dust, the NOAA HYSPLIT Saharan dust dispersion model was applied [22,23].

3. Results

3.1. PM_1 and PM_{10-1} mass concentrations

PM_1 mass concentrations at the palaces were comparable for both seasons (Fig. 2). During summer, the lowest levels were found at the P2 site. When comparing the concentrations at the palaces with those at

the outdoor reference site (R1), the trends are similar (Fig. 2). The similar indoor and outdoor temporal trend during winter shows that outdoor conditions regulate the amount of PM_1 at all palace interiors. During winter, precipitation was the main factor responsible for the observed variations. Days with extensive rain showers (up to 23 mm on day 8) were characterized with low PM_1 concentrations due to wash-out. During the summer campaign, daily PM_1 concentrations were correlated moderately with air temperature ($r=0.468$; $p<0.037$) and strongly with the absolute humidity ($r=0.828$; $p>0.0001$).

The amount of $PM_{10\text{-}1}$ varied considerably over seasons. This variation could be attributed to the suspension of mineral dust, which is favored under dry and hot summer conditions. The extent of soil suspension inside the palaces was sometimes considerably higher than at the corresponding reference sites (Fig. 2). During the summer campaign, each day an average of 5500 tourists visited the Nasrid palaces and the surrounding royal gardens. During the winter campaign only 2400–4100 tourists were counted per day. Although such a mass tourism could drastically affect the local concentration of coarse airborne particulate, no correlation could be found between the daily tourist count and the indoor $PM_{10\text{-}1}$ level. However, in the summer of 2009, about 21000 spectators visited the 'International Festival of Music and Dance', which is organized annually in Granada. On the 10th, 14th and 16th days of the summer campaign, rather intensive cultural events took place at the inner court of the "Carlos V

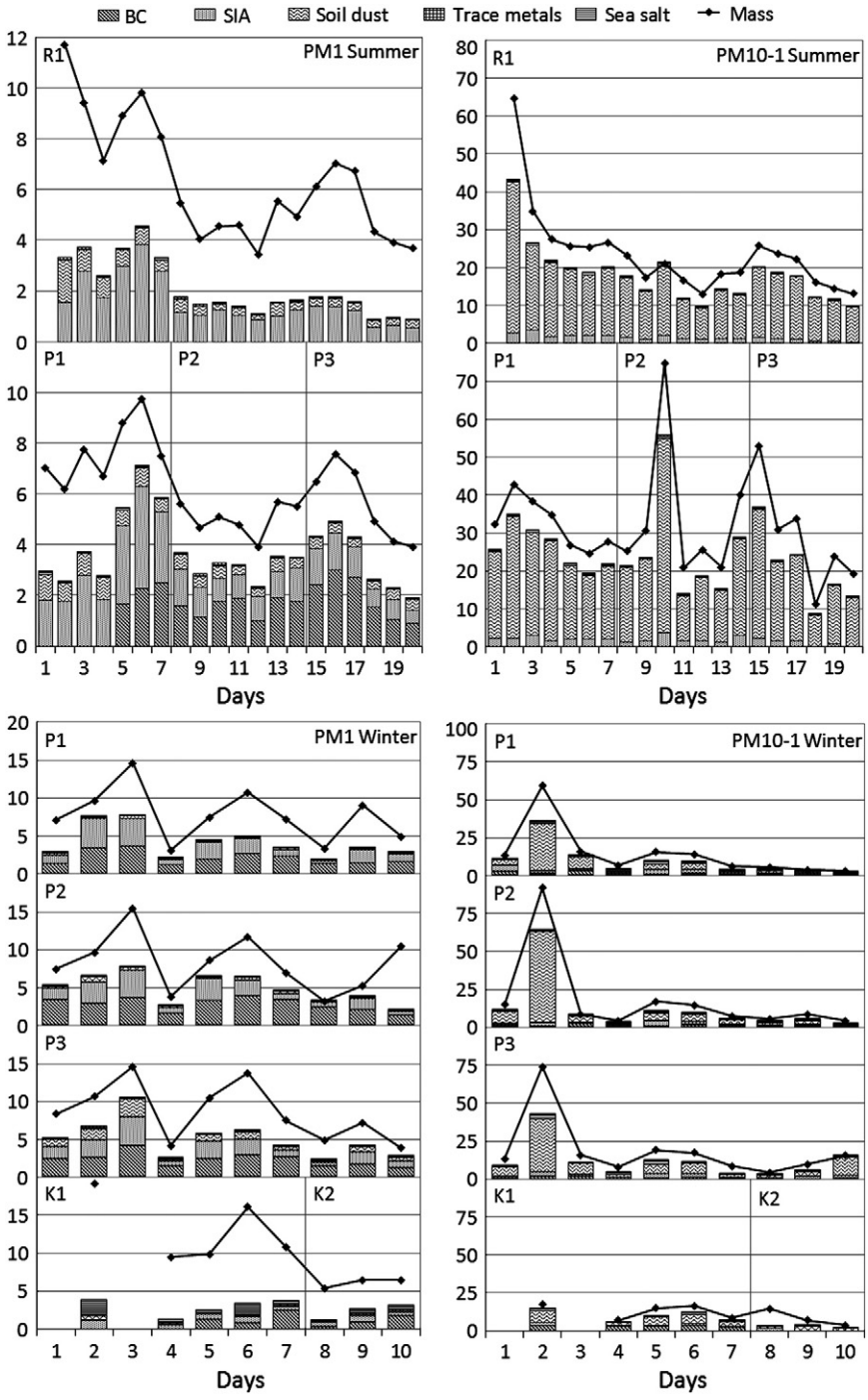

Fig. 2. Trends and mass balances for PM_1 and $PM_{10\text{-}1}$ ($\mu g\ m^{-3}$) collected during summer 2009 and winter 2010 – P1: the Hall of the two Sisters; P2: Royal Baths; P3: Hall of the Ambassadors; R1: reference site; K1: Cuesta del Chapiz; K2: Cuesta de Gomérez – Missing data: BC for summer $PM_{10\text{-}1}$; BC for summer PM_1 at R1; BC for summer PM_1 during day 1–4 at P1.

palace" (Fig. 1). It is likely that these events were responsible for the re-suspension of local soil dust, causing an increase in the $PM_{10\text{-}1}$ concentration at the Nasrid palaces (Fig. 2). On the 2nd day of the winter campaign, a steep increase in the $PM_{10\text{-}1}$ mass was observed inside the palaces. Since such a high concentration was not observed at the K1 site (Fig. 2), this aerosol mass increase might be due to the concurrent indoor activity (restoration/maintenance) in the vicinity of the palaces and the related re-suspension of dust.

3.2. Aerosol composition

Table 3 summarizes the average aerosol composition found at the Nasrid palaces. BC and SIA were the main components in PM_1, together contributing on average to more than 50% of the total mass. The $PM_{10\text{-}1}$ fraction was, especially in summer, extremely rich in soil dust components. The ion balance in the $PM_{10\text{-}1}$ fraction indicated a deficitin the total amount of analyzed anions ($Anions = 0.190 \times Cations - 16.0$; $r = 0.660$). Considering the high amounts of soil dust in $PM_{10\text{-}1}$, the missing anion was most likely CO_3^{2-} in the form of calcite ($CaCO_3$). When added to the total amount of anions in $PM_{10\text{-}1}$, the ion balance was completely restored ($Anions = 1.07 \times Cations - 0.999$; $r = 0.992$). It should be noticed that Ca^{2+} can also be present as gypsum ($CaSO_4 \cdot 2H_2O$), while CO_3^{2-} could be also dolomite ($CaMg(CO_3)_2$). However, considering the low concentrations of Mg^{2+} and SO_4^{2-} as compared to Ca^{2+}, one could neglect the presence of these salts, when estimating the amount of CO_3^{2-}.

During winter, PM_1 was rich in NH_4^+, having an average NH_4^+/SO_4^{2-} equivalent ratio of 1.4. Such a high NH_4^+ content suggests the contribution of NH_4NO_3 to the total mass of PM_1. Moreover, besides SO_4^{2-}, NH_4^+ was significantly correlated with NO_3^- too (Table 4). This correlation was even higher ($r = 0.945$; $p < 0.0001$), when using the excess of NH_4^+, i.e., the amount of NH_4^+ not corresponding to ammonium sulfate [24]. In summer, however, PM_1 particles were poor in NH_4^+ ($NH_4^+/SO_4^{2-} = 0.74$). Such a low NH_4^+ content suggests the absence of NH_4NO_3. The correlation coefficients show that ammonium sulfates were the only NH_4^+-salts present in PM_1 during summer. For $PM_{10\text{-}1}$, the correlations suggest the presence of sea salt (NaCl), as well as sodium nitrates and sulfates. Besides the aged sea salt, calcite and gypsum were also found in $PM_{10\text{-}1}$. The strong correlation between Mg^{2+} and CO_3^{2-}, as well as between Mg^{2+} and SO_4^{2-} suggests the presence of dolomite and Mg-rich sulfates, respectively, as found in reference [14].

Table 3
Average chemical composition (± standard error) of aerosols inside the Nasrid palaces (mg g^{-1} aerosol).

	Summer (n = 20)		Winter (n = 30)	
	PM_1	$PM_{10\text{-}1}$	PM_1	$PM_{10\text{-}1}$
Mass (μg m^{-3})	**6.1 ± 0.4**	**32 ± 3**	**8.2 ± 0.6**	**17 ± 4**
Black carbon	**308 ± 16**	**n.a.**	**317 ± 15**	**123 ± 13**
Soil dust	**55 ± 6**	**592 ± 13**	**17 ± 2**	**277 ± 26**
SiO_2[a]	19 ± 4	202 ± 9	2.8 ± 0.6	78 ± 7
Al_2O_3[a]	6 ± 1	70 ± 3	n.d.	22 ± 3
TiO_2[a]	0.4 ± 0.1	4.9 ± 0.2	n.d.	2.2 ± 0.2
$FeO + Fe_2O_3$[a]	6.4 ± 0.7	47 ± 1	2.9 ± 0.3	34 ± 2
Ca^{2+}	21 ± 4	70 ± 2	8 ± 1	38 ± 6
Mg^{2+}	1.0 ± 0.1	4.7 ± 0.2	0.5 ± 0.1	3.3 ± 0.4
CO_3^{2-}[b]	n.a.	194 ± 6	n.a.	98 ± 16
Sr	n.d.	0.45 ± 0.02	n.d.	0.36 ± 0.03
SIA[c]	**237 ± 17**	**56 ± 4**	**198 ± 13**	**130 ± 11**
NH_4^+	52 ± 5	n.d.	44 ± 4	n.d.
NO_3^-	8 ± 1	35 ± 3	70 ± 8	83 ± 7
SO_4^{2-}	177 ± 13	21 ± 2	84 ± 6	43 ± 4
Sea salt	**4.2 ± 0.6**	**11.1 ± 0.7**	**8.3 ± 0.9**	**67 ± 11**
Na^+	3.7 ± 0.4	8.3 ± 0.7	7.3 ± 0.7	40 ± 6
Cl^-	0.6 ± 0.2	2.7 ± 0.2	1.1 ± 0.3	27 ± 5
Trace metals	**5.2 ± 0.4**	**2.2 ± 0.1**	**3.7 ± 0.5**	**4.5 ± 0.6**
V	0.57 ± 0.06	0.12 ± 0.01	0.27 ± 0.03	0.31 ± 0.03
Cr	n.d.	0.10 ± 0.01	n.d.	n.d.
Ni	n.d.	0.06 ± 0.01	n.d.	0.19 ± 0.03
Cu	1.9 ± 0.2	0.90 ± 0.06	1.2 ± 0.2	2.0 ± 0.4
Zn	0.52 ± 0.06	0.46 ± 0.01	0.6 ± 0.1	0.68 ± 0.06
Pb	1.3 ± 0.1	0.52 ± 0.04	1.0 ± 0.2	1.1 ± 0.2
Unexplained	**391 ± 18**	**338 ± 14**	**456 ± 19**	**399 ± 26**

[a] Oxides calculated from element concentrations.
[b] Estimated from the anion deficit (cations – anions).
[c] Secondary inorganic aerosol.
n.d. – not detected.
n.a. – not applicable.

Table 4
Pearson's correlation coefficients indicating salt associations[a] between major anions and cations.

		NO_3^-		SO_4^{2-}		Cl^-		CO_3^{2-}[b]
		PM_1	$PM_{10\text{-}1}$	PM_1	$PM_{10\text{-}1}$	PM_1	$PM_{10\text{-}1}$	$PM_{10\text{-}1}$
Na^+	Summer	n.d.	**0.769**	n.d.	**0.539**	n.d.	0.211	0.452
	Winter	0.128	**0.549**	0.289	**0.665**	0.112	**0.716**	**0.664**
NH_4^+	Summer	n.d.	n.d.	**0.984**	n.d.	n.d.	n.d.	n.d.
	Winter	**0.905**	n.d.	**0.867**	n.d.	−0.218	n.d.	n.d.
Mg^{2+}	Summer	n.d.	0.475	0.474	**0.750**	n.d.	**0.600**	**0.895**
	Winter	0.435	**0.694**	0.179	**0.745**	−0.152	**0.538**	**0.836**
Ca^{2+}	Summer	n.d.	0.339	0.051	**0.817**	n.d.	**0.667**	**0.969**
	Winter	0.365	0.440	0.240	0.488	−0.038	0.312	**0.561**

[a] Salt association: $p < 0.001$ (bold).
[b] Estimated from the anion deficit (cations – anions).
n.d. – not detected.

4. Discussion

4.1. Local soil suspension and Saharan dust intrusion

According to the air-quality legislation of the European Commission (EC), days with PM_{10} concentrations above 50 μg m^{-3} are limited to 35 per year [25]. Due to increased soil dust suspension and regular intrusions of Saharan dust, many South European towns have difficulties in keeping this legislation [26]. For example, Lyamani and Bravo Aranda [27] reported 121 days in 2009 with PM_{10} exceedances of the EC limit for Granada. These increased PM_{10} levels were not only due to Saharan dust events (72 days), but were also due to the exceptionally intensive public construction works throughout 2009. In the present study, 2 out of 30 observation days were found with PM_{10} concentrations above 50 μg m^{-3}. Most of the increased PM_{10} mass could be attributed to local suspension of mineral dust with an EAD higher than 1 μm. Especially in summer, high loads of aluminum silicates and carbonates were received (Table 3) from the surrounding geological formation, consisting of quartzite, dolostone and limestone pebbles. Especially the construction of new underground train lines in Granada city was believed to contribute to the enhanced PM_{10} levels.

In Fig. 3, the evolution of a Saharan dust cloud, which passed over the Iberian Peninsula, is visualized by HYSPLIT during the first 7 days of the summer campaign, after which it dispersed over the Atlantic Ocean. Although the Sahara and Sahel deserts consist of many different petrologic regions, the mineral composition of their soil was found to be relatively constant [28]. Only the soil in the Northern parts of the Sahara was found to be significantly enriched in calcite and palygorskite [29]. However, when transported from the African continent, this regional specificity generally diminishes in a well-mixed body of Saharan aerosol. Some elemental ratios in aerosols could be used as a signature for Saharan soil. Although some Ca-based elemental ratios are popular for this purpose [30,31], they could not be used in an area dominated by calcareous soil. Average values for non-calcium based ratios are summarized in Table 5. Although the differences are small, Si-to-Fe and Ti-to-Fe ratios were significantly elevated during days with Saharan intrusion. In this period, the value for Ti-to-Fe was in good agreement with the ratio reported for

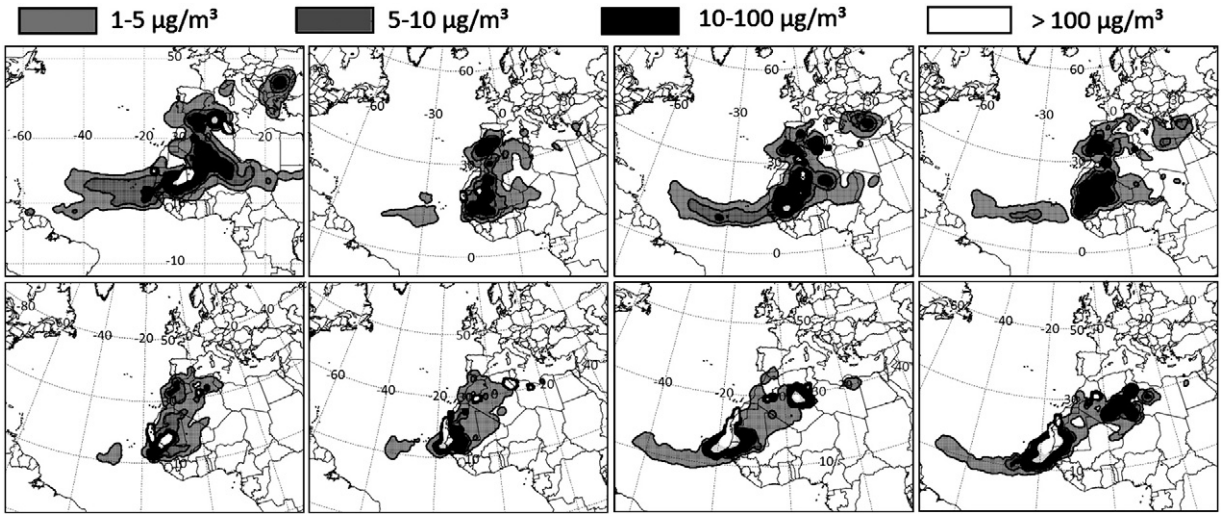

Fig. 3. Intrusion of a Saharan plume in the Iberian peninsula according to the NOAA HYSPLIT Saharan dust dispersion model – snapshots integrated between 23:00–00:00 UTC starting at 16th of June (top, left) until 23rd of June (bottom, right) 2009 – average concentrations between 0 and 100 m above ground level.

Saharan soil. On the contrary, the Si-to-Fe ratio was somewhat lower compared to the composition of Saharan dust. However, this could be explained by the gradual loss of coarse quartz particles with an increasing distance from the source [32].

4.2. SIA formation

As mentioned earlier, NH_4NO_3 in PM_1 was only observed during the winter campaign. Since the concentrations of NO_2 and NH_3 were quite comparable for both seasons (Table 6), the hot climate in summer (Table 1) likely promoted the vaporization of NH_4NO_3. On the contrary, ammonium sulfate in PM_1 was considerably present during both campaigns. The high summer concentrations for O_3 (Table 6) indicated serious smog conditions, in which SO_2 is rapidly, photo-chemically oxidized. This is in accordance with the low concentration of SO_2, which was often below the detection limit. The amount of ammonium sulfate is correlated strongly with the absolute humidity ($r = 0.746$; $p < 0.0001$), and demonstrates the importance of liquid phase reaction pathways in the oxidation of SO_2, and the subsequent formation of ammonium sulfate. The amount of strong acidity (H^+), captured in the particles as HSO_4^-, was estimated from the SO_4^{2-} and NH_4^+ concentrations assuming an ion-balance as proposed by Pathak et al. [24]. On average, the amount of H^+ was calculated to be 7 ± 0.5 neq m^{-3} (2–15 neq m^{-3}) and 0.7 ± 0.2 neq m^{-3} (0–6 neq m^{-3}) during summer and winter, respectively.

Since no NH_4^+ was detected in $PM_{10\text{-}1}$, SIA formed by homogeneous reactions were assumed to accumulate well below 1 µm EAD. SIA in $PM_{10\text{-}1}$ were formed via heterogenic reactions and were mainly present as aged sea salt. If it is assumed that all Na^+ originates from sea spray, the extent of Cl^- released from the aerosol phase can be estimated [33,34]. On average, about 70% and 90% of the expected Cl^- was lost during winter and summer, respectively. However, also the calcite and dolomite-rich soil acted as a sink for atmospheric H_2SO_4, which resulted in gypsum and Mg-rich sulfates.

4.3. Black carbon

In 2008, 626147 vehicles were officially registered in the province of Granada. From these, there were 421403 private cars, 112453 light and heavy duty trucks, 1131 buses and 3717 industrial tractors [35]. More than 90% of these buses, light and heavy duty vehicles, and tractors, and about 50% of these private cars were equipped with diesel engines. All together, these diesel fuelled vehicles consumed about 85% of the total fuel used for transportation in Granada [36]. Also, the domestic heating systems in the city are based on diesel combustion. However, considering the Mediterranean climate in Granada, domestic heating is considered to be a moderate source compared to mobile sources.

Fig. 4 shows a typical temporal pattern for the concentration of BC at the Nasrid palaces. Every day, the BC concentration started to increase around 9 am, reaching a maximum somewhere between 10 and 11 am, after which it dropped rapidly to the background level of 1 µg m^{-3}. A similar, but less sharp event occurred every evening between 7 and 10 pm. During weekdays, morning rush-hours

Table 5
Average mineral element ratios in $PM_{10\text{-}1}$ samples and literature data on African desert soils.

Ratio	Event[a]	$PM_{10\text{-}1}$				Sahel soil	Saharan soil	Saharan soil
		Mean $\pm \sigma_{95\%}$[b]	MD[c] $\pm \sigma_{95\%}$	t[d]	p[e]	1.5<d<12 µm	1.5<d<12 µm	d<50 µm
						[52]	[52]	[53]
Ti/Fe	SD	0.128 ± 0.005	0.020 ± 0.006	6.268	0.000	0.138	0.131	0.165
	SD-free	0.108 ± 0.004						
Si/Fe	SD	4.3 ± 0.2	0.5 ± 0.2	4.476	0.000	6.1	7.58	6.3
	SD-free	3.8 ± 0.1						
Si/Al	SD	2.60 ± 0.05	−0.04 ± 0.05	−1.970	0.103	3.7	4.06	3.92
	SD-free	2.68 ± 0.05						

[a] Saharan dust (SD) event (n = 7) and Saharan dust-free (n = 12) days during the summer campaign.
[b] 95% confidence interval.
[c] Mean difference.
[d] t-statistics.
[e] Significance.

Table 6
Average concentrations (±standard error) of gaseous pollutants at the Nasrid palaces (μg m^{-3}) [a].

Period	Site	O_3	NH_3	NO_2	SO_2
Summer 2009					
15/06-23/06	P1	181 (1)	6.6 (1)	16±1 (2)	n.d. (1)
	P2	85±9 (2)	8.9±0.2 (2)	15.4±0.6 (2)	n.d. (2)
	P3	229±7 (2)	8±1 (2)	17.5±0.2 (2)	1.018±0.003 (2)
23/06-30/06	P1	95±2 (2)	4.84±0.05 (2)	11.4±0.2 (2)	2 (1)
	P2	53±6 (2)	6.3±0.4 (2)	17.0±0.1 (2)	n.d. (1)
	P3	125±1 (2)	7.6±0.8 (2)	12.4±0.2 (2)	0.954±0.002 (2)
30/06-06/07	P1	103±4 (2)	6.3±0.1 (2)	14.0±0.8 (2)	0.9±0.1 (2)
	P2	56 (1)	8.3±0.2 (2)	17.3±0.2 (2)	n.d. (1)
	P3	120±11 (2)	9±1 (2)	14.574±0.004 (2)	1.2±0.1 (2)
15/06-06/07	P1	127±4 (3)	5.9±0.1 (3)	14±1 (3)	1.0±0.1 (3)
(Total)	P2	65±9 (3)	7.8±0.4 (3)	16.6±0.5 (3)	n.d. (3)
	P3	158±10 (3)	8±1 (3)	14.8±0.2 (3)	1.0±0.1 (3)
Winter 2010					
1/02-11/02	P1	62±8 (4)	7.2±0.3 (4)	16.9±0.7 (3)	n.d. (4)
(Total)	P2	28±3 (4)	7.7±0.2 (4)	8±1 (3)	n.d. (4)
	P3	60±1 (8)	6.8±0.2 (8)	18.3±0.4 (5)	1.1±0.1 (7)

[a] The number of parallel samples in parentheses. n.d. – not detected.

experienced the highest day-time concentrations, e.g., up to 15 μg m^{-3}, while during the evenings, peak concentrations of 3 μg m^{-3} were observed. On the weekends, the highest concentrations were recorded during the nightlife hours of Granada. Such a diurnal pattern was also observed by Lyamani and Bravo Aranda [27], it being typical for urban environments, where diesel-exhaust is the main source of BC. Despite the fact that traffic is minimized in the vicinity of the Alhambra monument, the observed BC concentrations are only slightly less compared to typical curbside concentrations found in other urban environments, for instance, Antwerp, Belgium [37].

At present, the gate of the pomegranates (Fig. 1) is closed for traffic, and all cars must approach the Alhambra monument from its eastern side. However, authorities of the city plan to open the gate in order to help tourists with finding their way to the monument. In order to evaluate the effect of such a decision, BC was monitored at the K2 side, in close proximity to the gate of the pomegranates, and at the K1 side, a similar steep street with dense traffic. Fig. 5 compares the BC concentrations for both sites. Concentrations at the K2 site were comparable as those found inside the Nasrid palaces, ranging from 0 to 15 μg m^{-3}, with a slightly elevated background concentration of 2 μg m^{-3}. At the Albayzin (K1), however, BC concentrations were extremely high, with an average of around 8 μg m^{-3}. Considering the similarity between both sites, opening the Gate of the Pomegranates for traffic could have serious implications for the levels of BC and other traffic-related pollutants in the vicinity of the Alhambra monument.

4.4. Anthropogenic sources of heavy metals

The PM_1 and PM_{10-1} particles were found to be significantly enriched in V, Ni, Cr, Cu, Zn and Pb (Table 7). According to the factor and correlation analyses, these metals could be divided into two distinct groups. The group corresponding to Ni and V represents most likely oil combustion sources. Since the V and Ni content of heavy oil is characteristic for the type of fuel, it is often used as a signature for specific oil combustion applications. Ratios of V-to-Ni in PM_1 are fairly approaching the value of 0.5 (Fig. 6), which is typically found in diesel combustion particles [9]. The increased scatter towards V-enriched particles in summer suggests the influence of additional, non-traffic sources. This is especially true for PM_{10-1} particles, which were found with V-to-Ni ratios ranging from 1 to 3 with an average of around 2. Despite the study of air-mass backward trajectories, no evidence could be found to attribute the V-to-Ni ratios to one or more specific industrial [38], or ship traffic related [39] sources. Therefore, in the non-industrialized area of Granada, the V and Ni concentrations in PM_{10-1} is considered to originate from a combination of various long-distance sources.

The common source for Cr, Cu, Pb and Zn could be less straightforward. A linear relation was found between the Cr-normalized

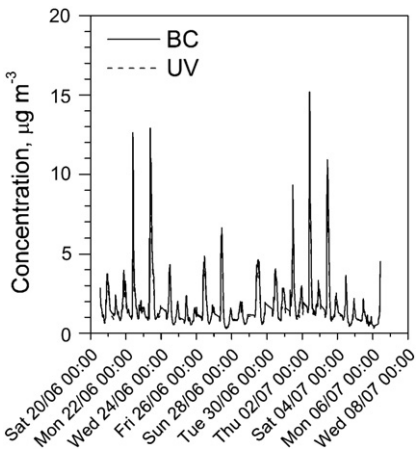

Fig. 4. Concentration trends of black carbon (BC) and UV-absorbing aerosols (UV) at the Nasrid palaces over the summer campaign in 2009 (times indicate 12 am).

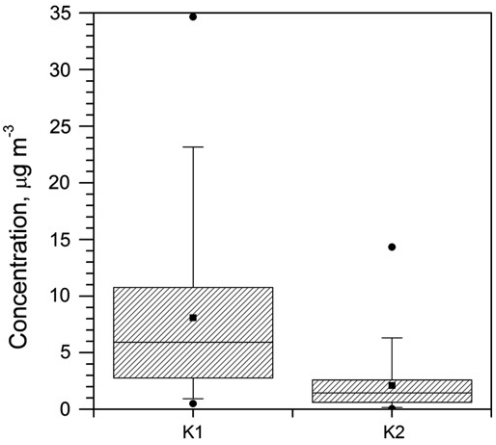

Fig. 5. Box-plot for black carbon concentrations at the curbside locations K1 and K2 – Box: 25th, 50th and 75th percentile; Whisker: 5th and 95th percentile; Circle: 1st and 99th percentile; Square: Mean.

Table 7
Average concentrations (C), crustal enrichment factors (EF_{UCC}), factor loadings (F), and correlation coefficients (r) for trace metals during the summer campaign[a] (n = 38).

	PM_1		PM_{10-1}		Factor analysis[c]		r[c,d]					
	C (ng m^{-3})	EF_{UCC}[b]	C (ng m^{-3})	EF_{UCC}[b]	F1 (52%)	F2 (27%)	Pb	Zn	Cu	Cr	Ni	V
V	4	242	4	6	0.112	**0.867**	0.081	0.372	0.052	0.106	**0.528**	
Ni	n.d.	188	3	12	−0.023	**0.875**	−0.035	0.251	0.016	−0.027		
Cr	5	1077	2	15	**0.783**	0.020	**0.524**	**0.735**	**0.547**			
Cu	11	2782	29	166	**0.920**	−0.015	**0.839**	**0.818**				
Zn	3	279	15	21	**0.911**	0.327	**0.743**					
Pb	8	2024	17	87	**0.895**	−0.039						

[a] Winter data were not considered due to the high number of non-detects (Table 2).
[b] For an element X, $EF_{UCC}(X) = (X_{PM}/Al_{PM})/(X_{UCC}/Al_{UCC})$; UCC: upper continental crust, from reference [54].
[c] Applied for trace metals in PM_{10}.
[d] Bold: $p<0.001$.
n.d. – not detected.

Cu and Pb concentrations in PM_{10} ([Cu:Cr] = 1.47 [Pb:Cr] + 1.24; r = 0.9555, $p<0.0001$). The slope of the regression curve suggested an average relative abundance for Cr:Cu:Pb close to 1:7:5. In relative amounts, this corresponds quite well to the tire wear emission reported by Hjortenkrans et al. [40] for the Stockholm area in 2005. It is to be noticed that the emission data reported by Hjortenkrans et al. [40] are based on tire sales figures, which could change over time and are not necessarily applicable to other tire markets. Although Cr, Cu and Pb are all present in tire tread, no records were found in the literature which used these metals as a tracer for tire wear. The calculation of Cu-to-Sb ratios, one of the most popular tracers for tire wear particles [41], was not possible due to the low sensitivity of the EDXRF method for Sb. However, besides the relative constant ratio, there are two other facts which favor the idea of tire wear as a common source for Cr, Cu and Pb: (1) Factor analysis accommodated Cr, Cu and Pb in the same principle component as Zn. Since ZnO is used in large amounts during the manufacturing process of tires, it supports the hypotheses that they all could be bound to tire debris particles; (2) Tire wear particles are formed by mechanical abrasion and are, therefore, expected to be mainly larger than 1 μm EAD. Since Cu, Pb and Zn were found at the highest concentrations in the PM_{10-1} fraction (Table 7), it is an extra motivation to assign tire wear as their major source.

4.5. Aerosols and their potential risks for conservation

Besides the effects of several reactive atmospheric gases, the deposition of environmental aerosols to historic buildings and structures could result in numerous physical and chemical weathering phenomena, and is considered to be a major threat to the conservation of CHIs. Deposition of hygroscopic salts on monuments attracts water and moisturizes the underlying material [1]. Dissolved salt components could migrate into porous materials, causing disruption of construction and decorative materials upon drying [42,43]. Moreover, moisture increases the mobility of diverse mixtures of transition metal oxides and mineral particles, which can act as a medium for surface reactions and stone decay [44]. The Royal Baths suffer from infiltrating rainwater, which transports salts through the walls, and has caused bulging cement and efflorescence on the walls. However, since the mortars and cements in the monument generally have a high porosity, humidity will probably be captured to a lesser extent, as compared to many other historical buildings [45].

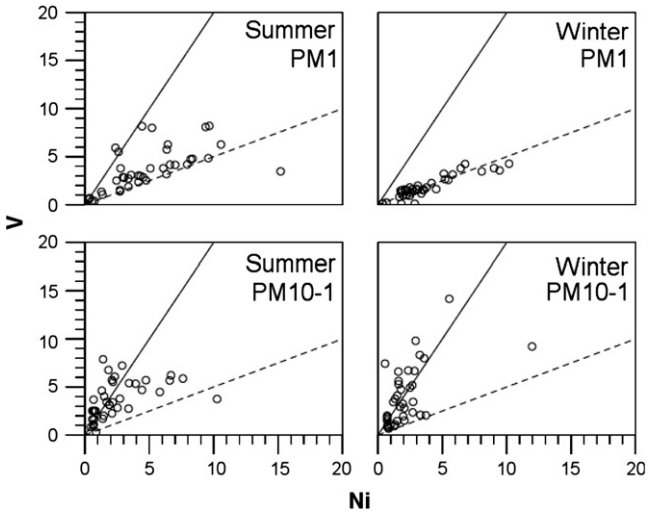

Fig. 6. Scatter plots for V and Ni concentrations (ng m^{-3}) illustrating the different V/Ni signatures for PM_1 and PM_{10-1} – solid line: V/Ni = 2; Dashed line: V/Ni = 0.5.

The major risk to the Alhambra posed by aerosols is the discoloration of polychromes, which are widely used in the stucco and carpentry artworks of the monument. The red color in the Alhambra polychromy is generally lost, and what remains either lacks intensity or is darkening and shows fissures [46]. Blackening of red lead (Pb_2O_3), one of the two red pigments in the Alhambra polychromy, evolves from solvolytic degradation and the formation of black platternite (PbO_2). On the other hand, the intensity of Pb_2O_3 will decrease due to the formation of white cerussite ($PbCO_3$) in the presence of alkali metal carbonates [47]. Considering the current state of the Pb_2O_3 pigment, both weathering processes were thought to occur extensively at the Alhambra, and could have been intensified by the deposition of hygroscopic salts and carbonates, which are dominant in the area.

Coarse, emerald-colored copper chloride grains were widely observed in the polychromes [46], and are generally known to be formed from sea salt weathering of the green malachite ($Cu_2(OH)_2CO_3$) pigment [48]. While most Cl^- escaped from the sea salts reaching the Alhambra monument, it is clear that the malachite pigment in the Alhambra has suffered from sea salt exposure.

Although blackening leads to a loss of the original quality of a CHI, there is an aesthetic threshold below which it could be publicly accepted. Brimblecombe and Grossi [49] reported that adverse public reactions were only triggered when a monument lost more than 35% of its reflectance. When the minimal time between cleaning events of a monument is 10 years, one could state that the annual averaged PM_{10} concentrations should not exceed 30 μg m^{-3} in order to maintain 35% of the monument's original reflection [50]. This is based on so-called dose-response functions between PM_{10} concentrations and the loss in reflectance on painted steel. It is to be noticed that the blackening of the stucco plasterworks, mortars and cements in the Alhambra monument [45,46] would have a different response to PM_{10} exposure. However, as a first approximation, these dose-response functions could be used to estimate the consequences of exposure to the currently determined PM_{10} levels. In summer, the

average PM_{10} concentration exceeded this threshold by about 30%, whereas in winter, the average level was only 25 μg m^{-3}. Since the higher PM_{10} concentrations in summer are mainly due to elevated concentrations of soil dust, it is not likely that they cause more blackening.

The potential hazards for blackening depends on the concentration of BC. Brimblecombe and Grossi [49] suggested that the exposure of stone buildings to elemental carbon (EC) levels above 2–3 μg m^{-3} triggered public aversion. The BC levels in this study –although not the same as EC – fall in this safe concentration range. However, this safe level could do more harm to relatively clean artworks, since the perceived lightness could be lost more drastically at the early stage of the exposure. It is to be noted that the construction of exposure guidelines for the protection of CHIs are often based on pure economic considerations and/or public perception, disregarding the historical and architectural values of the monument. Therefore, care must be taken when evaluating pollutant concentrations in this way. Since the decorative walls of the Nasrid palaces are not flat, but contain detailed curvatures and relief, the soiling process is enhanced, and makes them more difficult to clean. Moreover, the relief results in uneven blackening, which is often considered to be more offensive than a gradual, all over color change [51].

5. Conclusion

The palaces at the Alhambra monument were originally built to maximally integrate the surrounding nature and environment and to provide a refreshment shelter from the hot and dry climate of Granada. The rooms of the Nasrid palaces consist of high, arch-like entries and many opened windows. Consequently, the indoor concentrations of PM_1 and PM_{10-1} were observed to be fairly high, and followed closely the variations in the outdoor air quality. The PM_{10-1} aerosols were mainly composed of soil dust, rich in calcite, dolomite and silicates and contained considerable amounts of aged sea salts, especially $NaNO_3$. The carbonate rich soil originated mainly from local suspension, however, also North African dust contributed to the mineral aerosol content in summer. In the non-industrialized area of Granada, vehicular traffic was found to be the main source of PM_1, consisting mainly of ammonium sulfates and nitrates (the latter only during winter) and BC. Heavy metals were found to originate from diesel exhaust (V and Ni) and tire tread emissions (Cu, Cr, Pb and Zn).

Although the Alhambra brings prosperity and economic benefits to the Granada region, it should also be protected from the pressure of mass tourism. Recently, the city hall plans to help tourists with finding their way easier to the monument, by allowing vehicles to drive through the gate of the pomegranates and the Alhambra park. At present, the BC concentration close to the gate of the pomegranates is around an average of 2 μg m^{-3}. However, when the street is opened for traffic in the future, the BC concentration is expected to rise up to 8 μg m^{-3} or even higher, as found at a similarly steep and nearby street, with dense traffic. Such decisions could have a considerable impact on the levels of BC and other vehicle derived pollutants inside the Nasrid palaces, with major implications for their future conservation and the enjoyment of visitors to this famous monument.

Results from this work enabled the decision not to reopen Cuesta de Gomerez to general traffic. Although a final decision remains to be taken, the best available option appears to be a one-way limitation to electric micro-buses facilitating tourists access to the Alhambra. It is important to resolve the ongoing debate between the authorities of the Alhambra and the city hall of Granada, to define targeted strategies with respect to traffic sources, in order to preserve the Alhambra and its UNESCO world cultural heritage label.

Acknowledgement

The authors thank the research group RNM-179 (CICE, JA, Spain) and the 'Patronato de la Alhambra y Generalife' for making this research possible. Special thanks go to M. Urosevic and J. Romero-Pastor for their help in data acquisition. The authors gratefully acknowledge the NOAA Air Resources Laboratory (ARL) for the provision of the HYSPLIT transport and dispersion model and the READY website (http://www.arl.noaa.gov/ready. html) used in this publication.

References

[1] D. Camuffo, Microclimate for cultural heritage, Elsevier, Amsterdam, 1998.
[2] D.A. Dolske, Deposition of atmospheric pollutants to monuments, statues, and buildings, Sci. Total. Environ. 167 (1995) 15–31.
[3] M. Ferm, J. Watt, S. O'Hanlon, F. De Santis, C. Varotsos, Deposition measurement of particulate matter in connection with corrosion studies, Anal. Bioanal. Chem. 384 (2006) 1320–1330.
[4] C.M. Grossi, R.M. Esbert, F. Díaz-Pache, F.J. Alonso, Soiling of building stones in urban environments, Build. Environ. 38 (2003) 147–159.
[5] F. Monforti, R. Bellasio, R. Bianconi, G. Clai, G. Zanini, An evaluation of particle deposition fluxes to cultural heritage sites in Florence, Italy, Sci. Total. Environ. 334–335 (2004) 61–72.
[6] P. Pesava, R. Aksu, S. Toprak, H. Horváth, S. Seidl, Dry deposition of particles to building surfaces and soiling, Sci. Total. Environ. 235 (1999) 25–35.
[7] R. Van Grieken, F. Delalieux, K. Gysels, Cultural heritage and the environment, Pure Appl. Chem. 70 (1998) 2327–2331.
[8] T. Novakov, S.G. Chang, A.B. Harker, Sulphates as pollution particulates: catalytic formation on carbon (soot) particles, Science 186 (1974) 259–261.
[9] C. Rodriguez-Navarro, E. Sebastian, Role of particulate matter from vehicle exhaust on porous building stones (limestone) sulfation, Sci. Total. Environ. 187 (1996) 79–91.
[10] M. Ferm, F. De Santis, C. Varotsos, Nitric acid measurements in connection with corrosion studies, Atmos. Environ. 39 (2005) 6664–6672.
[11] A. Screpanti, A. De Marco, Corrosion on cultural heritage buildings in Italy: a role for ozone? Environ. Pollut. 157 (2009) 1513–1520.
[12] C.L. Shaver, G.R. Cass, J.R. Druzik, Ozone and the deterioration of works of art, Environ. Sci. Technol. 17 (1983) 748–752.
[13] S. Reis, R.W. Pinder, M. Zhang, G. Lijie, M.A. Sutton, Reactive nitrogen in atmospheric emission inventories, Atmos. Chem. Phys. 9 (2009) 7657–7677.
[14] V. Kontozova-Deutsch, C. Cardell, M. Urosevic, E. Ruiz-Agudo, F. Deutsch, R. Van Grieken, Characterization of indoor and outdoor atmospheric pollutants impacting architectural monuments: the case of San Jerónimo Monastery (Granada, Spain), Environ. Earth Sci. 63 (2011) 1433–1445.
[15] K. Gysels, F. Delalieux, F. Deutsch, R. Van Grieken, D. Camuffo, A. Bernardi, G. Sturaro, H.-J. Busse, M. Wieser, Indoor environment and conservation in the Royal Museum of Fine Arts, Antwerp, Belgium, J. Cult. Herit. 4 (2004) 221–230.
[16] K. Torfs, R. Van Grieken, Chemical relations between atmospheric aerosols, deposition and stone decay layers on historic buildings at the Mediterranean coast, Atmos. Environ. 31 (1997) 2179–2192.
[17] Z. Spolnik, K. Belikov, K. Van Meel, E. Adriaenssens, F. De Roeck, R. Van Grieken, Optimization of measurement conditions of an energy dispersive X-ray fluorescence spectrometer with high-energy polarized beam excitation for analysis of aerosol filters, Appl. Spectrosc. 59 (2005) 1465–1469.
[18] B. Horemans, A. Worobiec, A. Buczynska, K. Van Meel, R. Van Grieken, Airborne particulate matter and BTEX in office environments, J. Environ. Monit. 10 (2008) 867–876.
[19] P. Quincey, A relationship between Black Smoke Index and Black Carbon concentration, Atmos. Environ. 41 (2007) 7964–7968.
[20] ISO9835, Methods for measurement of air pollution — part 11: determination of a Black Smoke index in ambient air, 1993.
[21] Fondazione Salvatore Maugeri, Radiello, 2006, www.radiello.com (last access: 6th July, 2011).
[22] R.R. Draxler, G.D. Rolph, HYSPLIT (HYbrid Single-Particle Langrangian Integrated Trajectory) model access via NOAA ARL READY Website, NOAA Air Resources Laboratory, Silver Spring, MD, 2003, http://www.arl.noaa.gov/ready/hysplit4.html (last access: 6th July, 2011).
[23] G.D. Rolph, Real-time Environmental Applications and Display sYstem (READY) Website, NOAA Air Resources Laboratory, Silver Spring, MD, 2003, http://www.arl.noaa.gov/ready/hysplit4.html (last access: 6th July, 2011).
[24] R.K. Pathak, P.K.K. Louie, C.K. Chan, Characteristics of aerosol acidity in Hong Kong, Atmos. Environ. 38 (2004) 2965–2974.
[25] European Directive, Directive of the European Parliament and of the Council of 21 May 2008 on ambient air quality and cleaner air for Europe, 2008/50/EC, Off. J. Eur. Union, L152, 2008, pp. 1–44.
[26] T. Moreno, X. Querol, A. Alastueya, M. Viana, W. Gibbons, Exotic dust incursions into central Spain: implications for legislative controls on atmospheric particulates, Atmos. Environ. 39 (2005) 6109–6120.
[27] H. Lyamani, S.J.A. Bravo Aranda, Report on the air quality in Granada: year 2009 (in Spanish), Atmospheric physics group (GFAT), Andalusian center of the environment (CEAMA), Granada, 2010.

[28] T. Moreno, X. Querol, S. Castillo, A. Alastuey, E. Cuevas, L. Herrmann, M. Mounkaila, J. Elvira, W. Gibbons, Geochemical variations in Aeolian mineral particles from the Sahara-Sahel Dust Corridor, Chemosphere 65 (2006) 261–270.
[29] L. Schütz, M. Sebert, Mineral aerosols and source identification, J. Aerosol Sci. 18 (1987) 1–10.
[30] I. Chiapello, G. Bergametti, B. Chatenet, P. Bousquet, F. Dulac, E.S. Soares, Origins of African dust transported over the northeastern tropical Atlantic, J. Geophys. Res. 102 (1997) 13701–13709.
[31] I. Borbély-Kiss, Á.Z. Kiss, E. Koltay, G. Szabó, L. Bozó, Saharan dust episodes in Hungarian aerosol: elemental signatures and transport trajectories, J. Aerosol Sci. 35 (2004) 1205–1224.
[32] D.F. Gatz, J.M. Prospero, A large silicon-aluminum aerosol plume in Central Illinois: North African desert dust? Atmos. Environ. 30 (1996) 3789–3799.
[33] B. Horemans, A. Krata, A. Buczynska, A.C. Dirtu, K. Van Meel, R. Van Grieken, L. Bencs, Major ionic species in size-segregated aerosols and associated gaseous pollutants at a coastal site on the Belgian North Sea, J. Environ. Monit. 11 (2009) 670–677.
[34] J.J. Lin, Characterization of water-soluble ion species in urban ambient particles, Environ. Int. 28 (2002) 55–61.
[35] DGT, General yearly statistics 2008 (in Spanish), Ministerio del interior-Dirección general de tráfico, Madrid, 2008.
[36] Cores, Consumption of oil-based products, 2008, http://www.cores.es (last access: 6th July, 2011).
[37] B. Horemans, R. Van Grieken, Speciation and diurnal variation of thoracic, fine thoracic and sub micrometer airborne particulate matter at naturally ventilated office environments, Atmos. Environ. 44 (2010) 1497–1505.
[38] T. Moreno, X. Querol, A. Alastuey, J. de la Rosa, A.M. Sánchez de la Campa, M. Minguillón, M. Pandolfi, Y. González-Castanedo, E. Monfort, W. Gibbons, Variations in vanadium, nickel and lanthanoid element concentrations in urban air, Sci. Total. Environ. 408 (2010) 4569–4579.
[39] M. Viana, F. Amato, A. Alastuey, X. Querol, T. Moreno, S.G. Dos Santos, M.D. Herce, R. Fernández-Patier, Chemical tracers of particulate emissions from commercial shipping, Environ. Sci. Technol. 43 (2009) 7472–7477.
[40] D.S.T. Hjortenkrans, B.G. Bergbäck, A.V. Häggerud, Metal emissions from brake linings and tires: case studies of Stockholm, Sweden 1995/1998 and 2005, Environ. Sci. Technol. 41 (2007) 5224–5230.
[41] A. Thorpe, R.M. Harrison, Sources and properties of non-exhaust particulate matter from road traffic: a review, Sci. Total. Environ. 400 (2008) 270–282.
[42] C. Cardell, T. Rivas, M.J. Mosquera, J.M. Birginie, A. Moropoulou, B. Prieto, B. Silva, R. Van Grieken, Patterns of damage in igneous and sedimentary rocks under conditions simulating sea-salt weathering, Earth Surf. Proc. Land. 28 (2003) 1–14.
[43] T. Rivas, B. Prieto, B. Silva, J.M. Birginie, Weathering of granitic rocks by chlorides: effect of the nature of the solution on weathering morphology, Earth Surf. Proc. Land. 28 (2003) 425–436.
[44] J.J. McAlister, B.J. Smith, A. Török, Transition metals and water-soluble ions in deposits on a building and their potential catalysis of stone decay, Atmos. Environ. 42 (2008) 7657–7668.
[45] M.J. De la Torre López, P.E. Sebastián, G.J. Rodríguez, A study of the wall material in the Alhambra (Granada, Spain), Cem. Concr. Res. 26 (1996) 825–839.
[46] C. Cardell-Fernández, C. Navarrete-Aguilera, Pigment and plasterwork analyses of nasrid polychromed lacework stucco in the Alhambra (Granada, Spain), Stud. Conserv. 51 (2006) 161–176.
[47] E. Kotulanova, P. Bezdicka, D. Hradil, J. Hradilova, S. Svarcova, T. Grygar, Degradation of lead-based pigments by salt solutions, J. Cult. Herit. 10 (2009) 367–378.
[48] D.A. Scott, A review of copper chlorides and related salts in bronze corrosion and as painting pigments, Stud. Conserv. 45 (2000) 39–53.
[49] P. Brimblecombe, C.M. Grossi, Aesthetic thresholds and blackening of stone buildings, Sci. Total. Environ. 349 (2005) 175–189.
[50] J. Watt, D. Jarrett, R. Hamilton, Dose-response functions for the soiling of heritage materials due to air pollution exposure, Sci. Total. Environ. 400 (2008) 415–424.
[51] C.M. Grossi, P. Brimblecombe, Aesthetics of simulated soiling patterns on architecture, Environ. Sci. Technol. 38 (2004) 3971–3976.
[52] S. Castillo, T. Moreno, X. Querol, A. Alastuey, E. Cuevas, L. Herrmann, M. Mounkaila, W. Gibbons, Trace element variation in size-fractionated African desert dusts, J. Arid. Environ. 72 (2008) 1034–1045.
[53] C. Giuieu, A.J. Thomas, Saharan aerosols: from the soil to the ocean, in: S. Guerzoni, R. Chester (Eds.), The impact of desert dust across the Mediterranean, Kluwer Academic Publishers, Dordrecht, 1996, pp. 207–216.
[54] K.H. Wedepohl, The composition of the continental-crust, Geochim. Cosmochim. Acta 59 (1995) 1217–1232.